

Journal of Geophysical Research: Atmospheres

RESEARCH ARTICLE

10.1029/2017JD027823

Special Section:

Quantifying the emission, properties, and diverse impacts of wildfire smoke

Key Points:

- VIIRS mean FRP per pixel is fairly stable across swath, whereas MODIS mean FRP can increase by up to 300% at scan edge relative to nadir
- VIIRS FRP is generally comparable with contemporaneous MODIS FRP at continental scales and in most fire clusters
- FRP difference between VIIRS and MODIS retrievals is, on average, approximately 20% for 1-degree grid cells in most fire-prone regions

Correspondence to:

X. Zhang,
xiaoyang.zhang@sdstate.edu

Citation:

Li, F., Zhang, X., Kondragunta, S., & Csiszar, I. (2018). Comparison of fire radiative power estimates from VIIRS and MODIS observations. *Journal of Geophysical Research: Atmospheres*, 123, 4545–4563. <https://doi.org/10.1029/2017JD027823>

Received 29 SEP 2017

Accepted 4 APR 2018

Accepted article online 16 APR 2018

Published online 2 MAY 2018

Comparison of Fire Radiative Power Estimates From VIIRS and MODIS Observations

Fangjun Li¹ , Xiaoyang Zhang^{1,2} , Shobha Kondragunta³, and Ivan Csiszar³

¹Geospatial Sciences Center of Excellence, South Dakota State University, Brookings, SD, USA, ²Department of Geography, South Dakota State University, Brookings, SD, USA, ³NOAA/NESDIS/Center for Satellite Applications and Research, College Park, MD, USA

Abstract Satellite-based active fire data are a viable tool to understand the role of global fires in the biosphere and atmosphere. The Moderate Resolution Imaging Spectroradiometer (MODIS) sensors on Aqua and Terra satellites are nearing the end of their lives. The Visible Infrared Imaging Radiometer Suite (VIIRS) sensor on the Suomi National Polar-orbiting Partnership satellite and the subsequent Joint Polar Satellite System series is expected to extend the MODIS active fire record. Thus, understanding the similarities of and discrepancies between the two data sets during their overlap period is important for existing applications. This study investigated the dependence of the MODIS and VIIRS fire characterization capabilities on satellite view zenith angle and the relationship between the two sensors' fire radiative power (FRP) from individual fire clusters to fire data on continental and global scales. The results indicate that the VIIRS fire characterization capability is similar across swath, whereas MODIS is strongly dependent on view zenith angle. Statistical analyses reveal that the VIIRS and MODIS FRP relationship varies between different spatial scales. In fire clusters, MODIS and VIIRS FRP estimates are very comparable, except for large boreal forest fires where VIIRS FRP is approximately 47% smaller. At the continental scale, the contemporaneous FRP retrievals from MODIS and VIIRS are generally comparable and strongly correlated, but VIIRS FRP is slightly larger and their differences vary across seasons. At global $1^\circ \times 1^\circ$ grids, the FRP difference between the two sensors is, on average, approximately 20% in fire-prone regions but varies significantly in fire-limited regions.

1. Introduction

Satellite-detected active fire data have been widely used to study regional and global wildfire activity and its impacts on air quality and environmental changes during the last few decades (Csiszar et al., 2014; Flannigan & Haar, 1986; Giglio et al., 2003; Giglio et al., 2006; Prins & Menzel, 1992; Roberts & Wooster, 2008; Schroeder et al., 2014). One of the most important variables for characterizing wildfires is fire radiative power (FRP). This variable is retrieved from the radiance at the 4-μm band of satellite sensors and represents the instantaneous radiative energy that is released from actively burning fires. FRP has been extensively used as a proxy of fire intensity to characterize fire types (Roy & Kumar, 2017; Wooster & Zhang, 2004), fire behaviors (Smith & Wooster, 2005), and fire regimes (Archibald et al., 2013), to predict fire danger (Freeborn et al., 2016), and to investigate interactions among biomass burning, land cover dynamics, and hydrological cycles (Ichoku et al., 2016). More importantly, FRP is related to the rate of biomass combustion (Kaufman et al., 1998; Wooster et al., 2003) and the rate of emissions (Ichoku & Kaufman, 2005), which have been subsequently applied to estimate trace gas and aerosol emissions (Kaiser et al., 2012; Kumar et al., 2011; Vermote et al., 2009; Zhang et al., 2012).

FRP retrievals are available from multiple polar-orbiting and geostationary satellites. The Moderate Resolution Imaging Spectroradiometer (MODIS) instrument on board National Aeronautics and Space Administration (NASA)'s Earth Observing System (EOS) Aqua and Terra satellites, for example, has operationally detected active fires globally since 2000. The latest MODIS Collection 6 active fire product provides more scientifically reliable fire detections and FRP retrievals (Giglio, Schroeder, & Justice, 2016). However, Aqua and Terra MODIS sensors are aging and nearing the end of their lives. Continuity with Aqua MODIS is provided by the new generation moderate-resolution instrument called the Visible Infrared Imaging Radiometer Suite (VIIRS). The first VIIRS sensor is on board the Suomi National Polar-orbiting Partnership (Suomi NPP) satellite that was launched in 2011, and subsequent operational VIIRS sensors are planned for the series of Joint Polar Satellite System (Goldberg et al., 2013). (Note that the first operational VIIRS is flown on the NOAA-20 satellite, launched in November 2017. Fire data from this sensor are not included in this study.) Both Suomi NPP and

Aqua satellites cross the equator at approximately 1:30 a.m. (descending orbit) and 1:30 p.m. (ascending orbit) local times. Compared to the 1-km MODIS bands for fire detection, the VIIRS moderate resolution bands (M-bands) have a similar spectral configuration but higher spatial resolution (750 m; Cao et al., 2014). The higher spatial resolution in VIIRS relative to MODIS theoretically enables the detection of smaller and cooler fires (Csiszar et al., 2014). VIIRS also applies an onboard aggregation scheme to mitigate the increase in ground sampling distance with satellite scan angle, which strongly affects the detection capability of MODIS at off nadir (Cao et al., 2014; Freeborn et al., 2014; Peterson et al., 2013; Wolfe et al., 2002, 2013). To transition global fire observations from the MODIS era to the VIIRS era, it is essential to understand the similarities of and discrepancies between fire characterizations of the 1-km Aqua MODIS and 750-m VIIRS active fire products for application purposes. These comparisons currently exist only for a few sites between MODIS FRP and the early version VIIRS FRP (Oliva & Schroeder, 2015) that was derived based on the MODIS Collection 4 algorithm (Csiszar et al., 2014).

In this study, we compared 1 year of FRP retrievals from Aqua MODIS and Suomi NPP VIIRS observations globally. The newly operational 750-m VIIRS fire product is produced by NOAA (National Oceanic and Atmospheric Administration) using a modified algorithm of the MODIS Collection 6 (C6) active fire product (Giglio, Schroeder, & Justice, 2016); it has been available since April 2016 (Csiszar et al., 2016). This NOAA operational 750-m VIIRS active fire product is hereafter referred to simply as the VIIRS fire product. A comparison of the VIIRS product to the MODIS C6 active fire product should greatly improve our understanding of FRP characterizations for applications, such as estimating biomass burning emissions. To this end, we conducted the following analyses. First, the active fire detection data from VIIRS and MODIS products were pre-processed to correct duplicate detections in adjacent scans due to the bow tie effect and repeat detections that were observed from adjacent orbits. Then, the dependences of the two sensors' capabilities of detecting and characterizing fires on satellite view zenith angle (VZA) were investigated. Finally, comparisons between MODIS and VIIRS FRP estimates were conducted at the local fire cluster level over different ecosystems, at continental/global scale, and across latitudinal variation.

2. Data

2.1. MODIS Active Fire Data

The MODIS active fire product detects actively burning fires at the overpass times of the Terra and Aqua satellites (Giglio, Schroeder, & Justice, 2016). The 1-km Level-2 active fire product (abbreviated MOD14 for Terra and MYD14 for Aqua) provides for each fire pixel the detection time and coordinates (longitude and latitude) and confidence, FRP, brightness temperatures at the 4- and 11- μm bands, and satellite VZA (Giglio, Schroeder, & Justice, 2016). The detection confidence is quantified to a range of 0–100% and is further classified into three categories (high, nominal, and low; Giglio et al., 2003). The FRP in the latest MODIS C6 fire product is retrieved following the method developed by Wooster et al. (2003), which uses parameters including the radiances of the fire pixel at the 4- μm band, the radiances of the ambient nonfire pixels at the 4- μm band, area of the fire pixel, and a sensor-specific coefficient ($3.0 \times 10^{-9} \text{ W} \cdot \text{m}^{-2} \cdot \text{sr} \cdot \mu\text{m}^{-1} \cdot \text{K}^{-4}$; Giglio, Schroeder, & Justice, 2016). The MODIS C6 Level-2 active fire product records FRP retrievals in units of megawatts (per pixel).

The Level-2 MYD14 product is generated in an Aqua MODIS sensing geometry (Table 1; Wolfe et al., 1998, 2002). MODIS scans 10 lines of nominal 1-km pixel per mirror rotation over $\pm 55^\circ$ approximately every 1.477 s and each scan line is composed of 1354 pixels with a swath width of 2,340 km (Wolfe et al., 2002). The nominal pixel dimension increases from ~ 1 km at nadir to ~ 2.01 km along the track direction and ~ 4.83 km along the scan direction at the scan edge (Wolfe et al., 1998). Adjacent scans overlap each other up to 50% from scan angles of 24° to the scan edge (Wolfe et al., 2002), which can result in duplicate fire detections. Furthermore, duplicate fire detections can also result from the triangle-shaped point spread function (PSF) of MODIS (Freeborn et al., 2014). Moreover, MODIS can observe the same fires repeatedly from adjacent orbits at middle-to-high latitudes as its adjacent orbits overlap each other. In addition, MODIS misses observations inside the daily coverage gaps between adjacent orbits along the entire equatorial region between 30°S and 30°N latitudes (Figure 1a).

For the comparison with Suomi NPP VIIRS fire data, we obtained the Aqua MODIS C6 Level-2 active fire product (MYD14) and geolocation product (abbreviated MYD03 for Aqua) from NASA's Level-1 and

Table 1

Comparison Between MODIS and VIIRS Data in Sensing Geometry and the Algorithms Used for Active Fire Characterization

Sensor Parameters	MODIS (Aqua)	VIIRS (Suomi NPP)
Orbit altitude	~705 km	~840 km
Equator crossing time	1:30 a.m. and 1:30 p.m. local time	1:30 a.m. and 1:30 p.m. local time
Scan angle range	$\pm 55^\circ$	$\pm 56.28^\circ$
Swath width	2,340 km (1,354 pixels)	3,000 km (3,200 pixels)
Pixel dimensions	1 (nadir) to 2.01 km (along track)	750 (nadir) to 1.60 km (along track)
Swath width	1 (nadir) to 4.83 km (along scan)	750 (nadir) to 1.60 km (along scan)
Fire detection	B21 (3.929–3.989 μm)	M13 (3.987–4.145 μm)
Primary bands	B22 (3.940–4.001 μm)	M15 (10.234–11.248 μm)
Saturation temperature	B31 (10.780–11.280 μm)	M13 nominally saturates at 343 and 634 K at high- and low-gain settings, respectively; and M15 saturates at 363 K.
Active fire detection algorithm	MODIS Collection 6 (C6) active fire detection algorithm (Giglio, Schroeder, & Justice, 2016)	The VIIRS NDE fire algorithm keeps the core and main body of MODIS C6 algorithm, but it is slightly modified in separating fire pixel from background clear land pixels. To separate fire pixel from background land pixels, the VIIRS NDE uses the fixed thresholds test (see Giglio et al., 2003), while the MODIS C6 combines the same fixed thresholds test and a new dynamic threshold test (see Giglio, Schroeder, & Justice, 2016).
FRP calculation	Based on Wooster et al. (2003); MODIS sensor-specific coefficient ($3.0 \times 10^{-9} \text{ W} \cdot \text{m}^{-2} \cdot \text{sr} \cdot \mu\text{m}^{-1} \cdot \text{K}^{-4}$)	Based on Wooster et al. (2003); VIIRS sensor-specific coefficient ($2.88 \times 10^{-9} \text{ W} \cdot \text{m}^{-2} \cdot \text{sr} \cdot \mu\text{m}^{-1} \cdot \text{K}^{-4}$)

Note. MODIS = Moderate Resolution Imaging Spectroradiometer; VIIRS = Visible Infrared Imaging Radiometer Suite; Suomi NPP = Suomi National Polar-orbiting Partnership; FRP = fire radiative power; NDE = NPP Data Exploitation.

Atmosphere Archive and Distribution System (<https://ladsweb.modaps.eosdis.nasa.gov/>) for the period from April 2016 to March 2017. The geolocation product MYD03 was used to locate and extract the overlap areas between Aqua MODIS adjacent orbits.

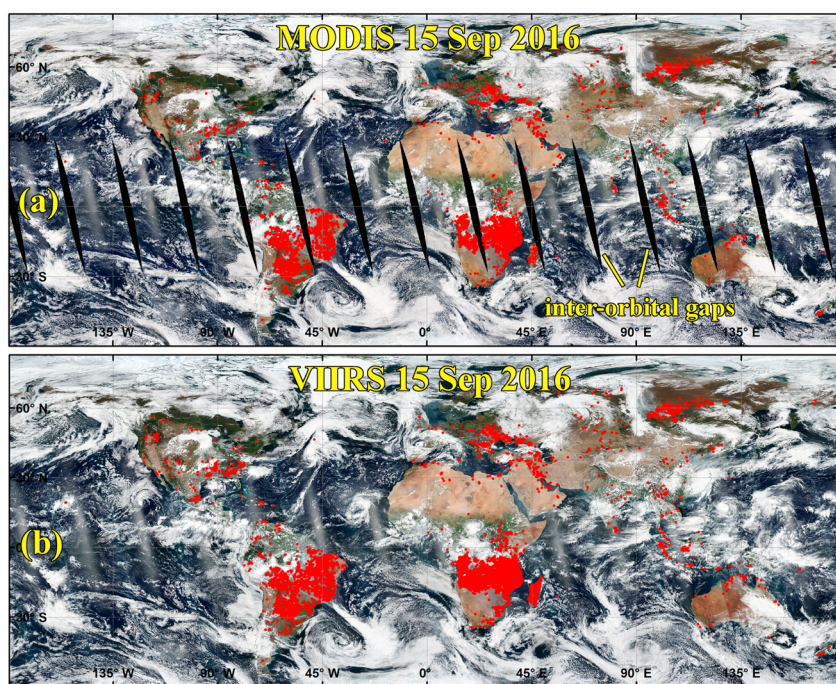


Figure 1. Global active fire detections from Aqua Moderate Resolution Imaging Spectroradiometer (MODIS) and Suomi National Polar-orbiting Partnership Visible Infrared Imaging Radiometer Suite (VIIRS) on 15 September 2016. (a) Daytime Aqua MODIS fire detections (red dots), which miss all fires burning inside the inter-orbital gaps (black narrow ellipses) in the low-latitude regions. (b) Daytime VIIRS fire detections (red dots), which provides daily full coverage of the globe.

2.2. VIIRS 750-m Active Fire Data

The newly operational NOAA VIIRS active fire product, the 750-m Suomi NPP Data Exploitation Level-2 active fire (NDEAF-L2), provides daily globally active fire data (Csiszar et al., 2016). The VIIRS NDEAF-L2 fire product is built on the modified active fire detection algorithm of the MODIS C6 active fire product (Giglio, Schroeder, Csiszar, & Tsidulko, 2016) and will extend to the Joint Polar Satellite System satellites (Csiszar et al., 2016). This product is also compatible with the 750-m VIIRS active fire products generated within NASA's Land Science Investigator-led Processing System. As with the MODIS active fire product, the VIIRS fire product contains for each fire pixel the detection time and coordinates (longitude and latitude) and confidence, FRP, brightness temperatures at 4- μ m and 11- μ m bands, and satellite VZA (Csiszar et al., 2016). The FRP (units: MW/pixel) recorded in the VIIRS NDEAF-L2 fire product is also retrieved based on the method proposed by Wooster et al. (2003). Although the algorithms for the VIIRS NDEAF-L2 fire product and the MODIS C6 active fire product are almost the same (Csiszar et al., 2016; Giglio, Schroeder, & Justice, 2016), MODIS and VIIRS sensors differ in the primary bands that are used for fire detection and FRP retrieval, their wavelengths, saturation temperatures, pixel sizes, and sensor-specific coefficient (Table 1).

The VIIRS NDEAF-L2 fire product is produced in the sensing geometry of the VIIRS M-bands (Table 1; Cao et al., 2014; Wolfe et al., 2013). The VIIRS M-bands sense 16 nominal 750-m pixel scan lines per scan with a scan angle range of $\pm 56.28^\circ$ from nadir approximately every 1.786 s, and each scan line is composed of 3,200 pixels that cover 3,000 km along the scan direction (Cao et al., 2014; Wolfe et al., 2013). Thus, the wider swath width, compared to MODIS, provides fully global coverage without gaps (Figure 1b). Coverage from adjacent orbits increasingly overlaps away from the equator toward higher latitudes, which can cause repeat detections of the same fires. Moreover, the nominal VIIRS pixels are generated using an aggregation scheme that determines the radiance value of a pixel from three samples in nadir along the scan direction (scan angle $<31.72^\circ$), from two samples in the middle zone of a scan (scan angle: 31.72° – 44.86°), and from one sample at the scan edge (scan angle $>44.86^\circ$), respectively. As a result, the growth rate of the VIIRS pixel size with view angle is largely reduced relative to MODIS observations (Wolfe et al., 2013). The pixel size of M-bands generally increases along the scan direction from nominal 0.75 km at nadir to ~ 1.6 km at the scan edge but decreases abruptly at the ends of aggregation zones (Wolfe et al., 2013). Moreover, the VIIRS onboard bow tie deletion algorithm removes two and four oversampling scan lines in the middle aggregation zone and at scan edge, respectively (Wolfe et al., 2013), thereby reducing duplicate fire detections between adjacent scans at off nadir. This deletion theoretically results in significantly fewer duplicate fire detections than MODIS.

This study collected the VIIRS NDEAF-L2 active fire product and the Moderate Bands Terrain Corrected Geolocation (GMTCO) product from the NOAA Comprehensive Large Array-Data Stewardship System (<https://www.class.ncdc.noaa.gov/>) for the period of April 2016 to March 2017. The GMTCO product was used to locate and extract the overlap areas between the Suomi NPP VIIRS adjacent orbits.

2.3. Land Cover Data

The MODIS land cover type was collected to determine the ecosystem types of fire occurrences. The primary land cover classification scheme in the MODIS land cover product (MCD12Q1) is provided by an International Geosphere-Biosphere Program (Friedl et al., 2010). This study used the most recent version of the MODIS land cover type product at a spatial resolution of 500 m in 2014 to examine the association between the fire detections from MODIS and VIIRS and the ecosystem types.

3. Methods

3.1. Correction of Interscan Duplicate Fire Detections

The duplicate fire detections between adjacent scans in MODIS and VIIRS fire products were extracted separately, and the associated FRP values were corrected. Fire pixels were considered as duplicate detections if they met the following three conditions: (1) Fires are detected at the same satellite view angles. (2) The time difference between any two fire observations is less than 8 s, which is because the same point on the Earth's surface could be sensed by up to three temporally adjacent scans at the scan edge during a time period of 4.431 s (the time of completing three scans is 3×1.477 s) for MODIS (Wolfe et al., 2002) and 5.358 s (3×1.786 s) for VIIRS M-bands, although ground-received VIIRS data are less likely to contain the same

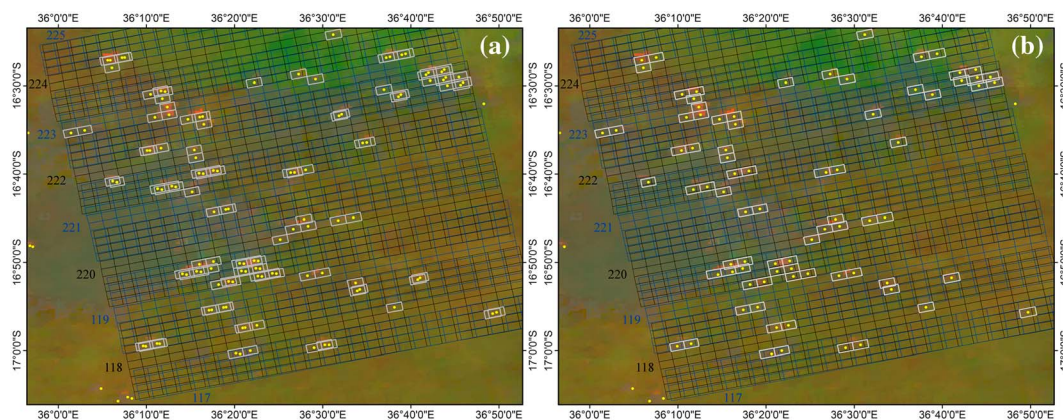


Figure 2. An example of correcting Moderate Resolution Imaging Spectroradiometer interscan duplicate fire detections for savanna fires in Southern Africa on 18 September 2016. (a) Before interscan correction. Nine temporally adjacent scans (117th–225th) sensed at 11:50 (UTC) are overlaid on a false-color composite image of 500 m Aqua Moderate Resolution Imaging Spectroradiometer band 7 (2,105–2,155 μm), band 2 (841–876 μm), and band 4 (545–565 μm), in which actively burning fires are denoted in red (or orange) color. Adjacent scans are in black and dark blue colors, respectively. Each scan has 10 scan lines and only 28 pixels at a view angle from 55° to 58° in each scan line (1,354 pixels) are shown here. Pixel boundaries are delineated by black or dark blue polygons, and the detected fire pixels are highlighted in white color with centers represented by yellow dots. Obviously, four scan lines in every two of adjacent scans overlap and the duplicate fire detections are those highlighted overlapping fire pixels with very close pixel centers. (b) After interscan correction.

surface point from all three adjacent scans due to the onboard deletion algorithm (Wolfe et al., 2013). (3) The distance between the centers of any two fire pixels is shorter than the along-track dimension of the fire pixels because adjacent scans primarily overlap each other along the track direction. For each pair of duplicate detections, one remained while the other was removed, and the average FRP was used as the corrected FRP value for the retained detection. Figure 2 shows an example of correcting MODIS interscan duplicate fire detections in nine temporally adjacent scans (117th–225th) at a satellite view angle from 55° to 58°, where a total of 40 pairs of duplicate fire detections were found and fully corrected.

3.2. Correction of Interorbital Duplicate Fire Detections

The duplicate detections of the same fires observed by Aqua MODIS and Suomi NPP VIIRS on adjacent orbits were extracted. Due to the overlap of among swaths from adjacent orbits at large VZA ($VZA > 40^\circ$), a fire could be repeatedly detected twice (by two adjacent orbits) across midlatitudes (Aqua MODIS: 30°S–61°S and 30°N–61°N, VIIRS: 54°S–54°N) and up to four times (by four adjacent orbits) across high latitudes (Aqua MODIS: 61°N–80°N, VIIRS: 54°N–80°N) during either daytime or nighttime everyday if the fire is intense and detectable at a large view angle with a large pixel size. Relative to MODIS, the VIIRS sensor has a much higher chance to detect the same fire from adjacent orbits because VIIRS M-bands have a generally consistent pixel size from nadir to the scan edge. To correct the interorbital duplicate detections, the daily overlap areas between adjacent orbits of each sensor were first built by spatially matching the associated swaths sensed from the adjacent orbits. Swath boundaries were constructed using the coordinates of the scan edges obtained from geolocation products (MYD03 for Aqua MODIS and GMTCO for VIIRS). Then, for every pair (or group) of the overlapping orbits, the fire pixels from one orbit inside the overlap area were extracted and buffered by a distance of the along-scan pixel dimensions at scan edge (4.83 km for MODIS and 1.6 km for VIIRS). For fire detections from the other orbit (or orbits), the detections located within the buffers were considered to be potential duplicate detections; otherwise, the detections outside the buffers were considered to be new fires. The buffered detections and their potential duplicate detections from either MODIS or VIIRS were then processed in the following three ways to determine whether the potential duplicate detections could be new fires. (1) Both the buffered and the potential duplicate fires remained if they were detected by both MODIS and VIIRS. (2) Only the fires detected by both MODIS and VIIRS remained if one of the sensors only observed either the buffered or potential duplicate fires. (3) Only the detections with smaller VZA remained if both the buffered and the potential duplicate fires were only detected from either MODIS or VIIRS. The selection of smaller VZA fire detection was based on the fact that the fire detection capability decreases as the view angle increases (see section 4.2). Additionally, all detections of new fires from the other orbits were also kept.

Table 2

Selected Fire Clusters at Five Typical Ecosystems in 13 Regions Across the Globe

Ecosystem	Region	Fire season ^a	Cluster number	Observing date	Observing difference	
					Time (minute)	VZA (degree)
Savannas	Northern Africa	November–January	45	2 November 2016	15	<10
	Southern Africa	July–September	75	22 August 2016	15	<15
	Australia	April–May, October–December	38	15 October 2016	0	<15
Tropical Rainforest	Amazon	August–September	100	7 and 15 September 2016	5–10	<10
	Southeast Asia	January–April	22	27 January and 5 May 2016	5–10	<10
	East Congo	August–October	40	11 July and 30 August 2016	10–15	<10
Boreal forest	North America	May–September	28	2 July 2016	15	<5
	Siberia	May–September	58	18 September 2016	10	<5
Broadleaf forest	Chile	December–January	98	21, 26, and 29 January 2017	5–20	<10
Croplands	Southeast United States	September–October	79	28 September and 06, 09, and 25 October 2016	5–20	<15
	Ukraine	July–August	20	13 and 26 July 2016	5–10	<15
	Northwest India	May and October	16	28 October 2016	0	<10

^aFire seasons were derived based on Giglio et al. (2006).

3.3. Comparison Between MODIS and VIIRS FRP Retrievals

To provide sufficient understanding of the similarity and discrepancy between MODIS and VIIRS FRP retrievals, we explored the FRP variations in four different ways. First, the dependence of MODIS and VIIRS FRP on VZA was examined and compared because of the differences in sensing geometry between the two sensors (Table 1). To ensure that both sensors sensed the fires contemporaneously in the same area, the Aqua MODIS granules were matched with the VIIRS granules temporally and spatially. Specifically, for each 5-min Aqua MODIS granule (based on MYD03), VIIRS granules (based on GMTCO) that temporally (± 5 min) and spatially (overlapping) matched the MODIS granule were first selected. Then, the fires detected inside the overlap areas between the MODIS granule and the matched VIIRS granules were considered as the contemporaneous fire detections because the variations of fires and atmosphere within ± 5 min could be negligible. This process was repeated for all MODIS and VIIRS granules from April 2016 to March 2017 globally. Finally, the contemporaneous fire detections were grouped with an interval of every 1° VZA, and the associated FRP values were then summed in each group for MODIS and VIIRS, respectively. The mean, minimum, and maximum FRP (per fire pixel) were further calculated for each sensor for comparisons.

Second, to understand the FRP variation in individual fire clusters, MODIS and VIIRS FRP estimates were compared for individual fire events that occurred during fire seasons in five typical ecosystems (savannas, tropical rainforests, boreal forests, broadleaf forests, and croplands; Table 2 and Figure 3). To minimize the effect of differences in observation time and VZA between MODIS and VIIRS, fire detections were extracted from those observed by both MODIS and VIIRS within a time difference of less than 20 min and a VZA difference of less than 15°. Using 20 min instead of 5 min was chosen to collect more contemporaneous fire detections with similar VZA and without cloud obscurations from both MODIS and VIIRS. A fire cluster was then manually enclosed using a polygon as shown in Figures 3d, 3g, 3j, 3m, and 3p. For visualization purposes, the extracted fire detections were overlaid with a false-color composite image of 500-m MODIS. The fire detections from MODIS and VIIRS were clustered around one or several fire pixels (red or orange color) on the MODIS false-color image. Figures 3b–3p present examples illustrating the fire clustering of active fire detections from MODIS and VIIRS in five ecosystems, where a large fire event could consist of several fire clusters. To select clusters representing various fire characteristics, a total number of 619 fire clusters were quantified from 13 regions globally (Table 2). For a fire cluster, VZAs were averaged and FRP retrievals were summed from all enclosed fire detections at each overpass for MODIS and VIIRS separately. Finally, the cluster level FRP estimates from the two sensors were compared for each of the five ecosystems using the reduced major axis (RMA) regression method that minimizes error in both dependent and independent variables (Smith, 2009). RMA regression has been widely used to compare measurements or estimates of the same

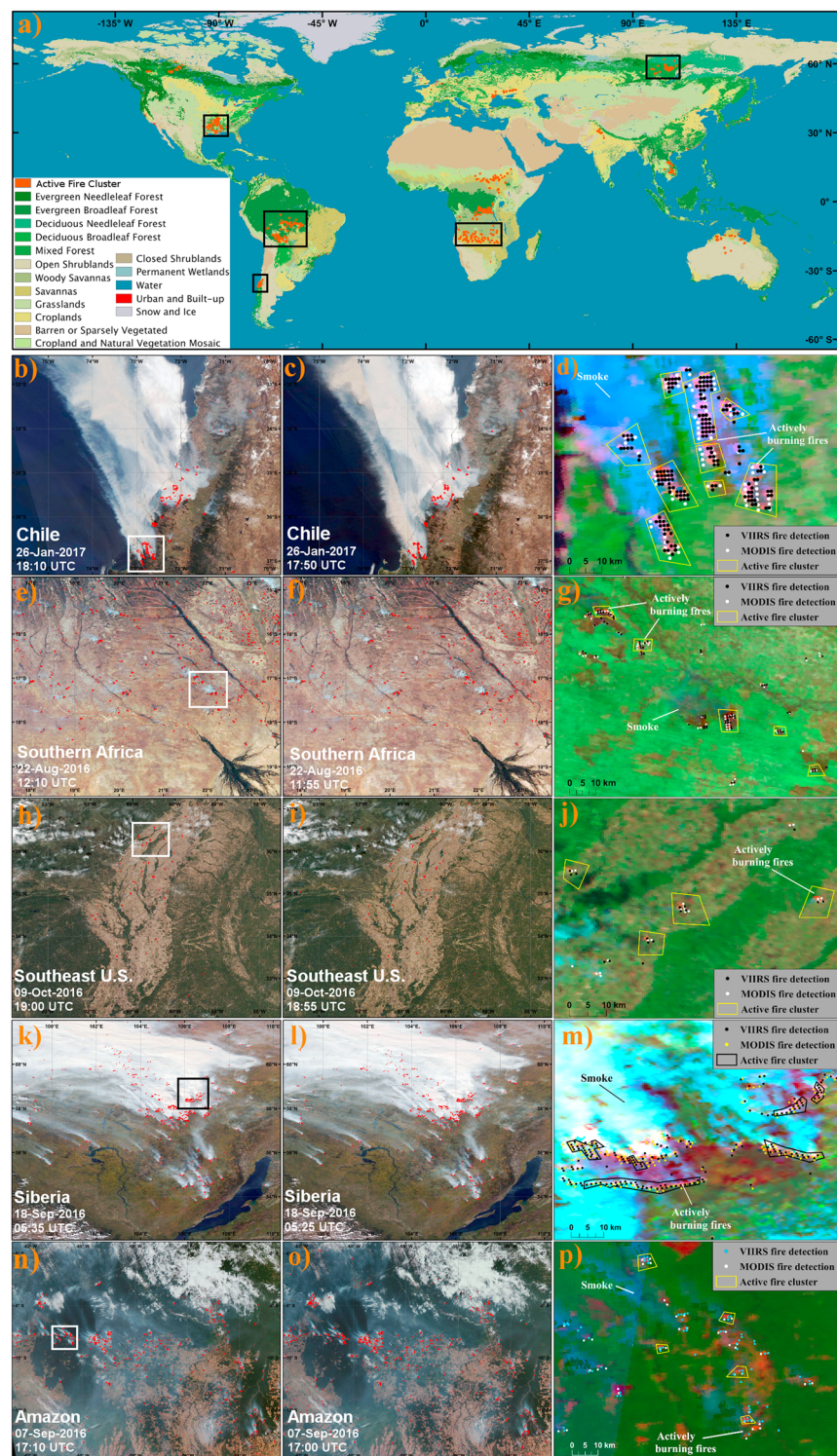


Figure 3. Fire clusters in five typical ecosystems selected globally. (a) The distribution of 619 fire clusters over 13 regions of savannas, tropical rainforest, boreal forests, broadleaf forest, and croplands (Table 2). The five black squares highlight the example regions used for illustrating fire clustering in the bottom panel. (b–p) Examples of active fire detections by Moderate Resolution Imaging Spectroradiometer (MODIS; b, e, h, k, and n) and Visible Infrared Imaging Radiometer Suite (VIIRS; c, f, i, l, and o) in one region of every ecosystem, and several manually selected fire clusters (d, g, j, m, and p) in the areas delineated by the white or black contours in the first column (b, e, h, k, and n). Fire clusters (highlighted by yellow or black polygons) were overlaid with the 500-m MODIS false-color composite image of bands 7-2-4 in which actively burning fires are in red (or orange).

geophysical or biophysical variable by different instruments (Boersma et al., 2009; Cohen et al., 2003; White et al., 2009). In this comparison, the fitted line was forced through the origin because both sensors observed the same fire clusters (or events) contemporaneously. The Pearson's correlation coefficient (r) was also calculated as an indicator of correlation between FRP estimates from the two sensors.

Third, the discrepancy between MODIS FRP and VIIRS FRP was investigated at a continental scale. The extracted contemporaneous fire detections (an overpass difference of within ± 5 min) from the two sensors, which were obtained from MODIS and VIIRS granules described in the first paragraph of this section, were separated into two groups by daily overpass times: (1) an early morning group at approximately 1:30 a.m. local time (nighttime fires) and (2) an early afternoon group at approximately 1:30 p.m. local time (daytime fires). For each of the daytime and nighttime groups, FRP retrievals of all contemporaneous fire detections from each sensor in the same day were summed separately for the six continents (North America, South America, Europe, Africa, Asia, and Australia). Then, the continental FRP estimates from the two sensors were statistically compared using the RMA regression. The regression intercept was kept because MODIS and VIIRS were not always able to detect the same fires.

Fourth, the discrepancy between MODIS FRP and VIIRS FRP was also investigated spatially at 1° grid cells across the globe. This comparison used all fire detections with the correction of duplicate detections for the following two reasons. First, the samples for statistical analyses were too small in a grid cell and were unrepresentative if only using the contemporaneous fires detections (within ± 5 min) from MODIS and VIIRS overpasses. Indeed, because of the overpass time shifts between MODIS and VIIRS orbits, the contemporaneous detections occurred approximately 1 day every 8 days (or ~ 45 days during an entire year) in the same area. For an area with a fire season approximately 1–2 months, the contemporaneous fire detections only appeared in 3–7 days. In that case, the extracted contemporaneous fires detections could be unable to represent the fire activities. Second, the operational biomass burning emission products, including the Quick Fire Emissions Dataset (QFED; Darmenov & Silva, 2015), the Global Fire Simulating System (GFAS; Kaiser et al., 2012) and the Blended Global Biomass Burning Emissions Product from MODIS, VIIRS, and Geostationary Satellites (GBBEPx; Zhang et al., 2014), estimate emissions at grid cells based on daily mean FRP flux (units: $\text{W} \cdot \text{m}^{-2} \cdot \text{s}^{-1}$) that is calculated using daily MODIS FRP retrievals. Therefore, the use of all corrected fire detections helps to understand the uncertainties of estimating emissions from VIIRS and MODIS FRP retrievals. To explore the spatial pattern of the FRP discrepancy, the VIIRS-to-MODIS FRP ratio was calculated at 1° grid cells by adopting a method that has been developed in previous studies (Ellicott et al., 2009; Freeborn et al., 2009; Roberts et al., 2015; Roberts & Wooster, 2008; Vermote et al., 2009; Wooster et al., 2015), in which the FRP ratio was applied to compare the FRP retrievals between MODIS and the Spinning Enhanced Visible and Infrared Imager across Africa and between Aqua MODIS and Terra MODIS across different regions globally in a temporal interval of 1 week, 1 month, or 1 year. In this study, the corrected fires detections from the two sensors were separately gridded into 1° grid cells. Then, the VIIRS-to-MODIS FRP ratio was calculated for every grid cell as

$$\phi_{\text{FRP}} = \frac{\sum_{i_{\text{VIIRS}}=1}^{n_{\text{VIIRS}}} \text{FRP}_{i_{\text{VIIRS}}}}{\sum_{i_{\text{MODIS}}=1}^{n_{\text{MODIS}}} \text{FRP}_{i_{\text{MODIS}}}} \quad (1)$$

where ϕ_{FRP} is the VIIRS-to-MODIS FRP ratio, i_{VIIRS} and i_{MODIS} are the indices of fire pixel number, and n_{VIIRS} and n_{MODIS} are the total number of corrected fire pixels in a grid cell for VIIRS and MODIS observations, respectively, from April 2016 to March 2017. Note that ϕ_{FRP} was not calculated for grid cells where fewer than 10 fire pixels were observed by either MODIS or VIIRS during the period.

Fire pixel density (units: count/km²) from VIIRS fire detections was also estimated at 1° grid cells to locate frequent fire occurrences and to investigate its influence on the VIIRS-to-MODIS FRP ratio. The fire pixel density was obtained by dividing the total fire pixel number by the area of the grid cell following the methods presented in Giglio et al. (2006) and Ichoku et al. (2008).

Finally, the VIIRS-to-MODIS FRP ratio was calculated using equation (1) for all corrected fire detections that were binned by every 5° latitude to explore the MODIS and VIIRS FRP discrepancy along the latitudinal direction.

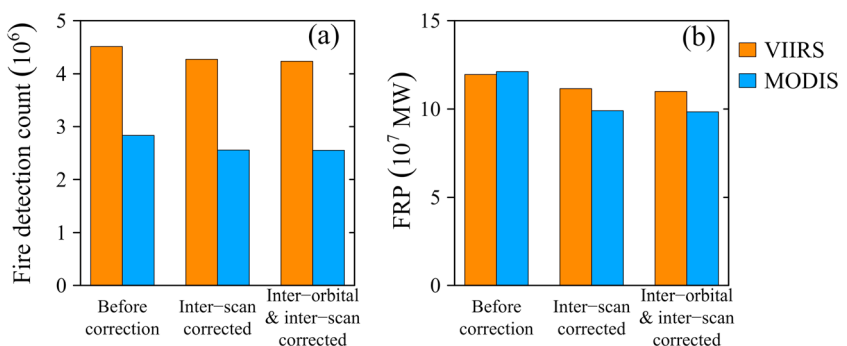


Figure 4. Fire detection count and cumulative fire radiative power (FRP) estimates before and after corrections of interscan and interorbital duplicate detections during the period from April 2016 to March 2017. (a) Total count of fire detections. (b) Cumulative FRP. VIIRS = Visible Infrared Imaging Radiometer Suite; MODIS = Moderate Resolution Imaging Spectroradiometer.

4. Results

4.1. Effect of Duplicate Detections on FRP Estimates

Duplicate fire detections from interscans (between adjacent pixels at off nadir and adjacent scans) account for considerable FRP overestimates (Figure 4). These duplicate detections account for as much as 9.8% of total fire count, which account for 18.3% of cumulative Aqua MODIS FRP at a global extent. This is similar to the finding from (Freeborn et al., 2014). In contrast, for VIIRS fire detections during the same period, duplicates account for up to 5.4% of the total fire count and 6.7% of the cumulative FRP.

The effect of the interorbital duplicate fire detections on FRP estimates is very limited (Figure 4). The repeat MODIS detections inside the overlap areas between the adjacent Aqua orbits only make up 0.18% of the total count of Aqua MODIS detections, which merely account for 0.54% of the cumulative FRP. For VIIRS detections, the interorbital duplicate detections account for only 0.8% of the total detections and contribute to 1.3% of the cumulative FRP.

4.2. Dependence of FRP Retrievals on Satellite VZA

A comparison of the fires that were contemporaneously detected by MODIS and VIIRS shows that the capability of detecting fire across swath is largely variable for MODIS but is relatively consistent for VIIRS (Figure 5). The MODIS fire count decreases by 67%, whereas the MODIS mean FRP per detection increases by 300% from 22 to 90 MW as VZA increases from nadir to 60° (Figures 5a and 5b). This variation is attributed to the gradual increase in pixel dimensions as VZA increases (Table 1). In contrast, the VIIRS fire count and mean FRP increase minimally by approximately 100% and 110%, respectively, from nadir to scan edge. The peaks of VIIRS fire count (also mean FRP) occur at approximately VZAs of 38° and 54° due to the change in pixel size associated with the onboard aggregation scheme (Wolfe et al., 2013). The discrepancy due to the sensing geometry difference between MODIS and VIIRS can also be seen in the minimum FRP per detection (in 1° VZA bin) that increases from 1.8 to 3.6 MW for VIIRS and 2.5 to 17.0 MW for MODIS as VZA increases from nadir to 60° (Figure 5c). The maximum FRP per detection from both VIIRS and MODIS shows large variation but generally increases as VZA increases from nadir to 60° (Figure 5c). In general, the sum of FRP estimates from VIIRS fire detections is 11% larger than that from MODIS fire detections, except for VZAs between nadir and +20° (Figure 5d).

4.3. Fire Cluster FRP

VIIRS and MODIS FRP estimates are mostly comparable in fire clusters, although there is a dependency on the host ecosystem (Figure 6). VIIRS FRP differs from MODIS FRP by approximately 1% in croplands and savannas. The regression coefficient (slope) suggests that the cluster FRP estimates from the two sensors are statistically similar in these two ecosystems with a Pearson's r of 0.72 and 0.81 (Figures 6a and 6b). The MODIS and VIIRS FRP estimates are also similar in broadleaf forests and tropical rainforests with a Pearson's r that is larger than 0.9. The cluster VIIRS FRP is approximately 13% larger than MODIS FRP, although a few cluster samples show larger MODIS FRP estimates in broadleaf forests (Figure 6c). A small difference is observed in tropical rainforests where the cluster VIIRS FRP is approximately 8% smaller than MODIS FRP (Figure 6d).

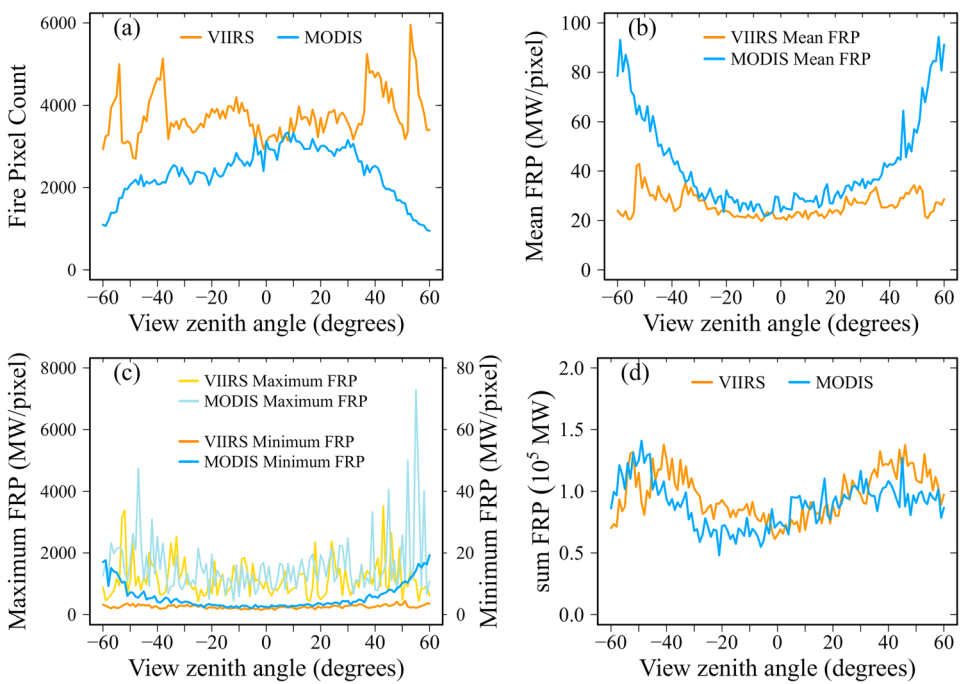


Figure 5. Variations of fire pixel count, sum fire radiative power (FRP), mean FRP, the minimum, and maximum FRP with view zenith angle for the daytime fires contemporaneously detected from Moderate Resolution Imaging Spectroradiometer (MODIS) and Visible Infrared Imaging Radiometer Suite (VIIRS) from April 2016 to March 2017 globally. (a) Fire detection count, (b) mean FRP per fire detection, (c) the maximum and minimum FRP per fire detection (the minimum FRP is on the right Y axis), and (d) sum of fire FRP, in every 1° view zenith angle bin.

However, the cluster VIIRS FRP estimates differ greatly from MODIS FRP in boreal forests (Figure 6e). Samples with a cluster FRP estimate less than 1,000 MW are evenly distributed around the 1:1 line. Nevertheless, MODIS FRP is 47% larger than VIIRS FRP in large cluster FRP samples (cluster FRP > 1,000 MW).

Although the samples have a VZA variation of 0° to 60°, the relationship of cluster FRP between MODIS and VIIRS retrievals does not show any dependence on VZA. This pattern appears in all five ecosystems.

4.4. Continental-Scale FRP

The continental-scale daily daytime FRP retrieved from VIIRS and MODIS contemporaneous fire detections is highly correlated (Pearson's $r \geq 0.98$) in all six continents although slight differences exist (Figure 7). In South America, Asia, and Australia, most of the samples are distributed around the 1:1 line with a slope that is close to one and a relatively small intercept, which suggests that the continental FRP differences between MODIS and VIIRS are generally very small. However, an FRP difference is observed in some periods during the year in South America and Australia. For instance, the VIIRS FRP estimates are slightly lower than MODIS FRP during August and September in South America (a time period dominated by deforestation fires) but are slightly larger from October–November (a time period dominated by savanna fires) in Australia.

Furthermore, although the regression slope between MODIS and VIIRS FRP estimates is close to one in Africa, the fitted line shifts toward the VIIRS side with a moderate systematic bias (Figure 7d). This indicates that the VIIRS FRP estimates are overall larger than MODIS FRP. The seasonal variation shows that the VIIRS FRP estimates are larger than MODIS FRP in the periods from January to April and August to December (time periods dominated by savanna fires in Northern and Southern Africa) but are smaller from May to July (a time period dominated by forest fires in central Africa rainforest).

The regression lines also show that VIIRS FRP is overall larger than MODIS FRP in North America and Europe (Figures 7a and 7c). In North America, the difference is mostly associated with agricultural burning and grassland fires that primarily occur during the period from March to June in Mexico, as well as the central and southeastern United States. In Europe, the overall larger FRP estimates of VIIRS than MODIS is related to agricultural burnings that begin in June and end in October.

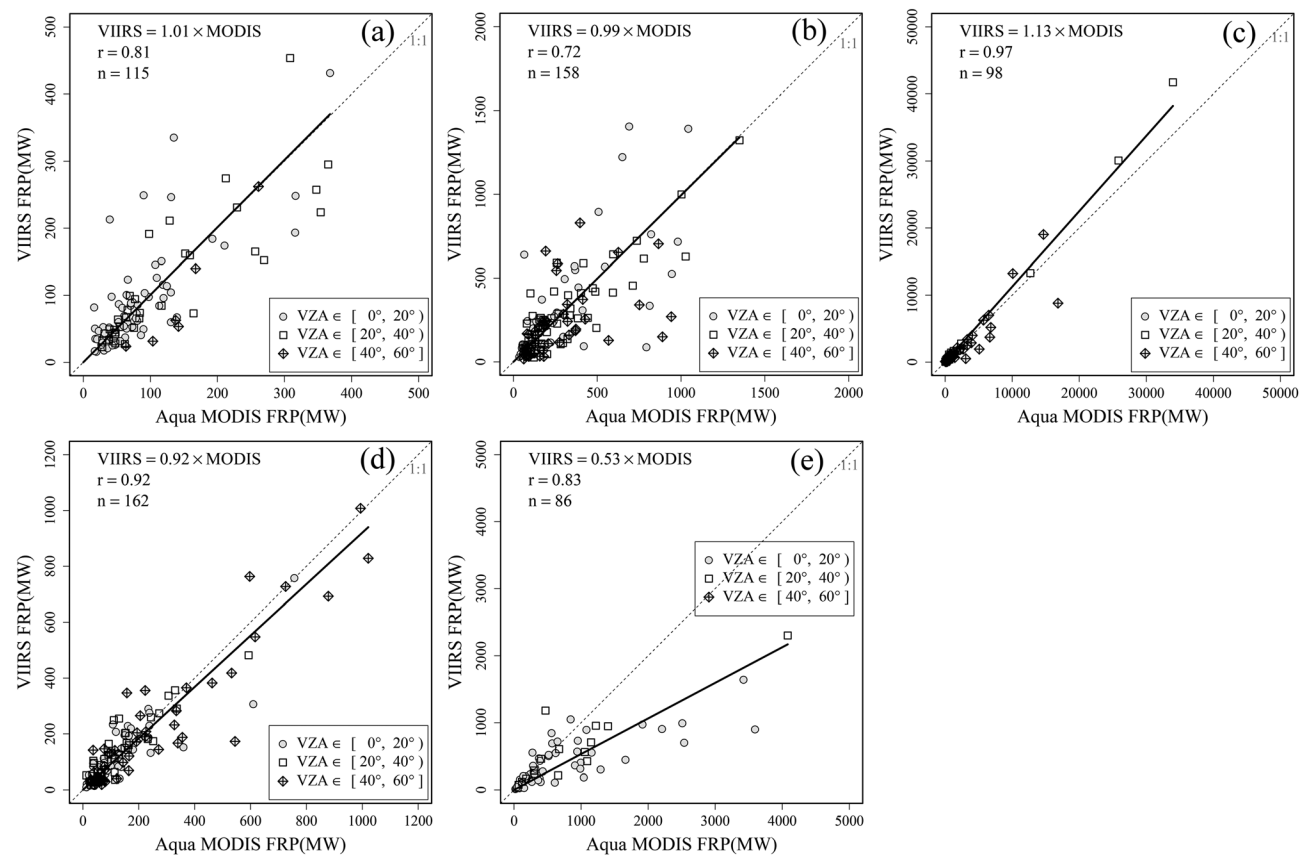


Figure 6. Comparison of fire cluster fire radiative power (FRP) between Visible Infrared Imaging Radiometer Suite (VIIRS) and Moderate Resolution Imaging Spectroradiometer (MODIS) estimates in five typical ecosystems. (a) Croplands, (b) savannas, (c) broadleaf forests, (d) tropical rainforests, and (e) boreal forests. Each sample represents one fire cluster. All samples are separated into three groups by the associated view zenith angle (VZA; 0°–20°, 20°–40°, and 40°–60°) and are represented using different symbols. The solid line is the fitted line and the dashed line is the 1:1 line.

Compared to the daytime continental FRP, the nighttime continental FRP estimates are much smaller and less correlated (Figure 8). This difference is likely associated with the much smaller and cooler fires that occur at night compared to daytime fires. Among the six continents, VIIRS FRP is overall larger than MODIS FRP in Europe and Africa but smaller in North America, South America, and Australia. However, FRP estimates between the two sensors are very comparable in most samples in Asia.

4.5. Spatial Pattern of Global FRP

The difference between VIIRS FRP and MODIS FRP estimates at grid cells is small in fire-prone regions (Figure 9). The fire-prone regions are quantified using the VIIRS fire pixel density showing large values for frequent fire occurrences (Figure 9a). These regions are mainly distributed in tropical and subtropical climate zones (including Africa, most parts of South America and Central America, Southeast Asia, and northern Australia). In fire-prone tropical and subtropical regions with a VIIRS fire pixel density that is larger than 0.05 count per square kilometer in a year, the VIIRS-to-MODIS FRP ratio shows that the VIIRS FRP estimates are, on average, 20% larger than MODIS FRP at the grid level (Figures 9b and 9c). The VIIRS-to-MODIS FRP ratio is consistent in fire-prone regions, whereas it varies dramatically in fire-limited regions where the VIIRS fire pixel density is less than 0.02 count per square kilometer in a year (Figure 9c). The FRP ratio in fire-limited regions is not representative because the fire sample size is too small.

The VIIRS-to-MODIS FRP ratio presents the spatial variation of the difference between VIIRS and MODIS FRP estimates in the grid cell across the globe (Figure 9b). At low latitudes, the VIIRS FRP estimates are larger than MODIS FRP in most regions that are dominated by agricultural and savanna fires, including croplands in Mexico, India, and Pakistan, and savannas in most of Africa and eastern South America. In contrast, VIIRS

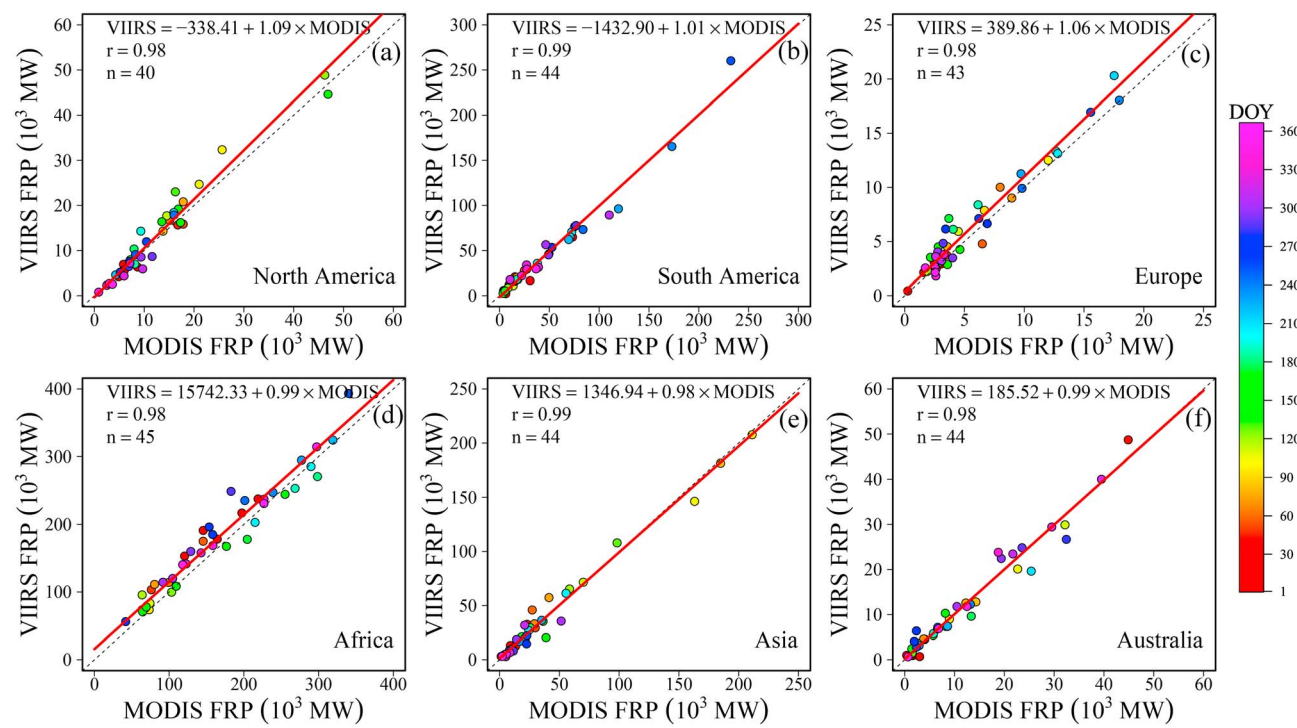


Figure 7. Comparisons of daily continental fire radiative power (FRP) estimates from daytime fire detections contemporaneously sensed by Visible Infrared Imaging Radiometer Suite (VIIRS) and Moderate Resolution Imaging Spectroradiometer (MODIS) during the period from April 2016 to March 2017 in six regions: (a) North America, (b) South America, (c) Europe, (d) Africa, (e) Asia, and (f) Australia. The solid line (red) is the fitted line and the dashed line is the 1:1 line. The date (day of year or DOY) of each sample is represented by different colors (see legend on the right).

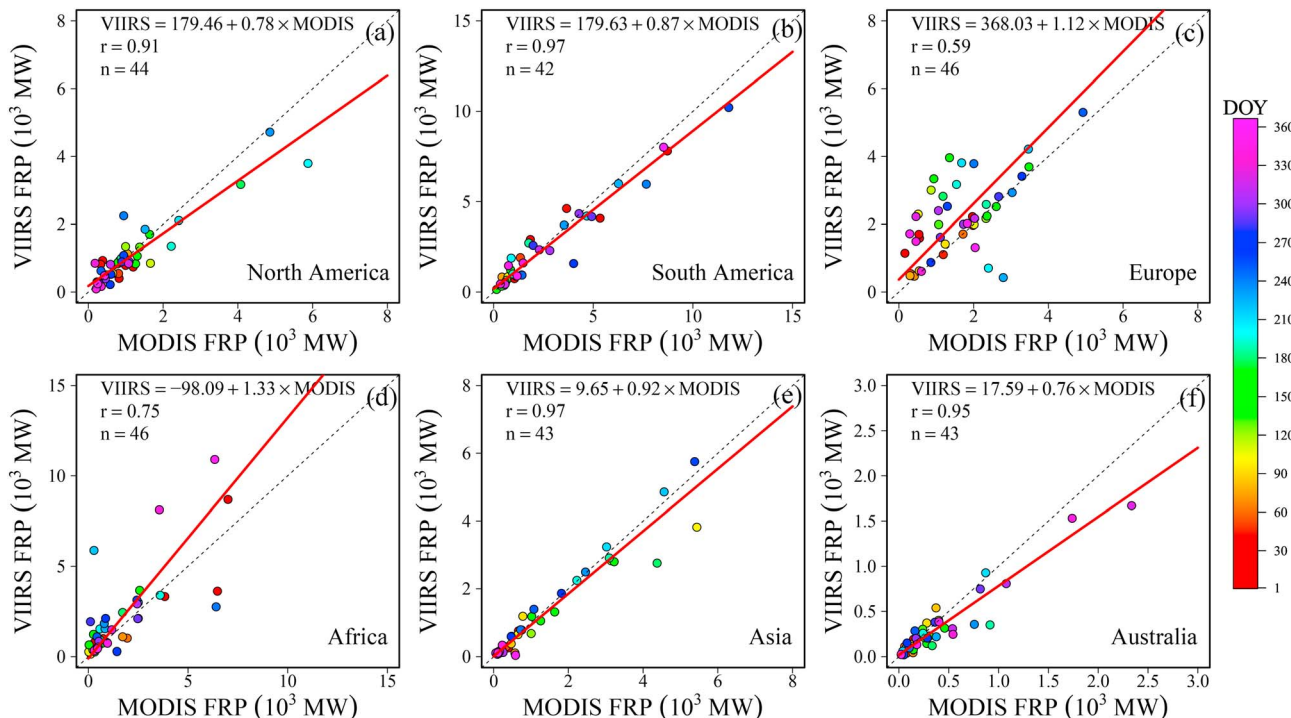


Figure 8. The same as in Figure 7 but for nighttime contemporaneous fire detections. FRP = fire radiative power; VIIRS = Visible Infrared Imaging Radiometer Suite; MODIS = Moderate Resolution Imaging Spectroradiometer; DOY = day of year.

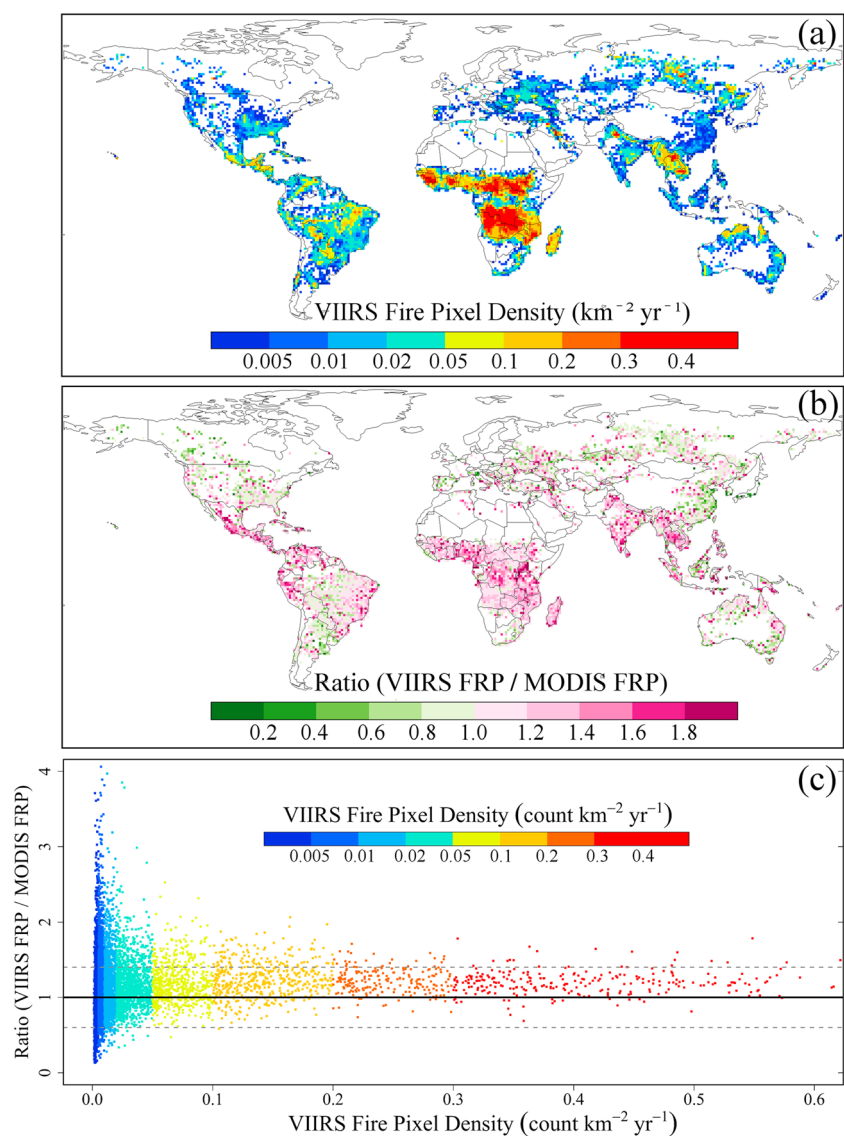


Figure 9. The Visible Infrared Imaging Radiometer Suite (VIIRS) fire pixel density and the VIIRS-to-Moderate Resolution Imaging Spectroradiometer (MODIS) fire radiative power (FRP) ratio at $1^\circ \times 1^\circ$ grid cells during the period from April 2016 to March 2017. (a) The VIIRS fire pixel density (units: $\text{count} \cdot \text{km}^{-2} \cdot \text{yr}^{-1}$), (b) the VIIRS-to-MODIS FRP ratio, and (c) the VIIRS-to-MODIS FRP ratio in grid cells as a function of VIIRS fire pixel density that is colored for different ranges. The solid line and the upper and lower dashed lines in (c) are ratio values of 1.0, 1.4, and 0.6, respectively.

FRP is mostly smaller than MODIS FRP in tropical forest fire regions, including areas in transition zones from savannas to rainforests in South America and on some Indonesian islands. In midlatitudes, the FRP ratio varies considerably within a local region, indicating that the relationship between VIIRS FRP and MODIS FRP is very complex. At high latitudes, VIIRS FRP is generally smaller than MODIS FRP. For instance, in the boreal forests where large and intense fires frequently occur during summer months (July–September) in North America and northern Asia, VIIRS FRP is as much as 40% smaller (much smaller in a few grids) than MODIS FRP although VIIRS FRP is slightly larger in a small portion of grids.

4.6. Latitudinal FRP Distributions

VIIRS and MODIS fire counts vary substantially with latitude (Figure 10a). At low latitudes between 30°S and 30°N , the annual count of fire detections accounts for over 88% of the total global fire detections. The fire count peaks in the equatorial savannas where the fire season spans from August to October in the Southern Hemisphere and from December to the following March in the Northern Hemisphere. However,

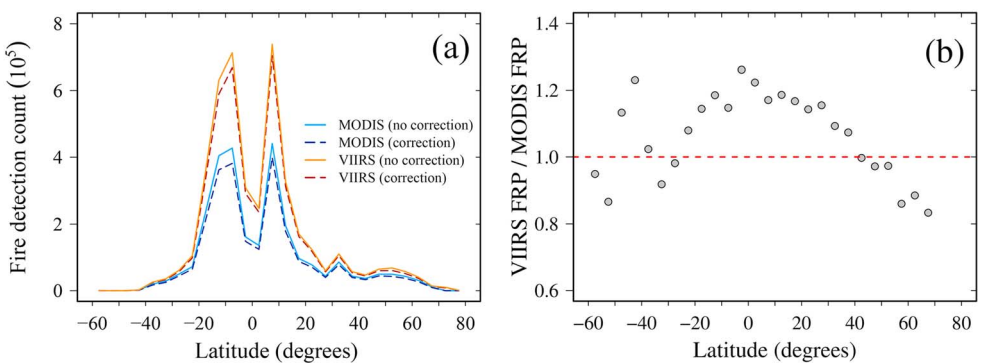


Figure 10. Variations in fire detection count and the Visible Infrared Imaging Radiometer Suite (VIIRS)-to-Moderate Resolution Imaging Spectroradiometer (MODIS) fire radiative power (FRP) ratio with latitude during the period from April 2016 to March 2017. (a) The annual total count of fire detection aggregated every 5° latitudes, where solid and dashed lines represent fire detection data before and after corrections of duplicate detections, respectively. (b) The VIIRS-to-MODIS FRP ratio at every 5° latitudes using the corrected fire detection data. The red dash line shows a ratio value of one, indicating VIIRS and MODIS FRP estimates are equal.

the fire count dips around the equator where tropical rainforests are dominant and fires are less frequent than in tropical savannas. Nevertheless, the fire count at middle-to-high latitudes decreases rapidly. This latitude-dependent pattern is the same for both the raw fire detections and the corrected fire detections. Relatively speaking, the count of the corrected VIIRS fire detections is much larger than that of the corrected MODIS fire detections, particularly in tropical regions (70% larger), which is mainly attributed to the difference in pixel size between the two sensors.

VIIRS FRP is generally larger than MODIS FRP at low latitudes but is smaller at middle-to-high latitudes (Figure 10b). For the corrected fire detections, the VIIRS-to-MODIS FRP ratio indicates that VIIRS FRP is, on average, approximately 16% larger than MODIS FRP in the tropical zone (30°S–30°N). In the Northern Hemisphere, VIIRS FRP is less than MODIS FRP up to 3% in midlatitudes (30°N–50°N) but up to 18% at high latitudes (55°N–70°N) where boreal forest fires frequently occur. In the Southern Hemisphere, the FRP ratio varies from 0.8 to 1.22 at middle-to-high latitudes where fire activity is relatively limited.

5. Discussion

The interscan duplicate fire detections could result in considerable FRP overestimation, while the interorbital duplicates have very limited effect on FRP estimates. The interscan duplicates in the MODIS fire data increase the cumulative FRP by approximately 2 times more than those in the VIIRS fire data. This suggests that VIIRS fire data are less affected by the interscan duplicate detections than MODIS fire data. The difference is mainly because (1) the combined VIIRS PSF in the 3- and 2-pixel aggregation zones is much less likely to produce duplicate detections than the triangle-shaped MODIS PSF (Cao et al., 2014) and (2) the onboard deletion of oversampled scans in VIIRS largely reduces the bow tie effect and leads to very limited overlaps between VIIRS adjacent scans (Wolfe et al., 2013). For MODIS, however, the interscan duplicate detections result in higher overestimation of the cumulative FRP than total fire count (Figure 4). This is because the interscan duplicate detections mainly occur at large VZA where mean FRP per detection is several times that of the mean FRP at nadir (Figure 5c). In contrast, the interorbital duplicates have very limited or negligible contributions to FRP estimates for both VIIRS and MODIS, although the impacts are stronger on the VIIRS than MODIS fire data because of the wider swath width and large overlap areas in VIIRS (Table 1; Wolfe et al., 2002, 2013).

Geometry differences between MODIS and VIIRS sensors could result in considerable discrepancies in fire detection and characterization across swath. The MODIS fire counts decrease quickly as VZA increases, whereas the FRP per count, especially the mean and minimum, increases greatly. This pattern coincides with the variation of MODIS pixel size. In contrast, VIIRS fire detections and FRP per count show limited variations, particularly in large VZAs at off nadir. This difference in fire detections between the two sensors is because of their different onboard aggregation schemes (Wolfe et al., 2013). Indeed, the large increase in MODIS pixel size across swath greatly decreases the MODIS detection capability, but the slight variation in VIIRS pixel size across swath marginally reduces the VIIRS detection capability, which is clearly demonstrated by the variation of the minimum FRP across swath (Figure 5c). Moreover, the difference in the mean FRP per count is mainly

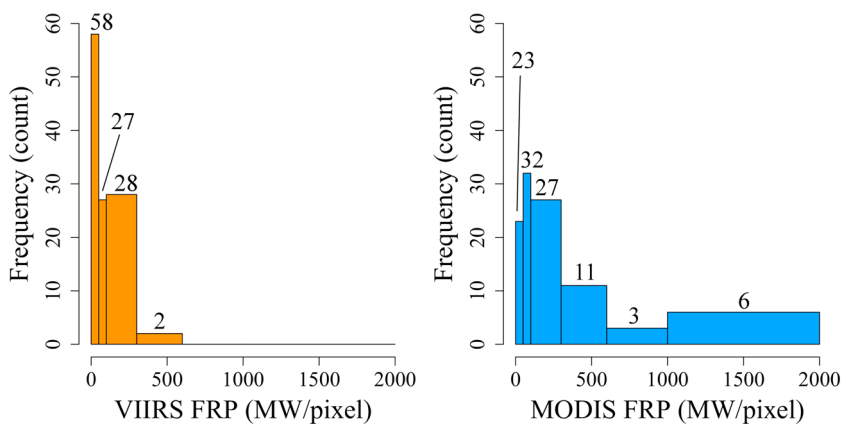


Figure 11. Distributions of the contemporaneous Visible Infrared Imaging Radiometer Suite (VIIRS) and Moderate Resolution Imaging Spectroradiometer (MODIS) fire detections in fire clusters against fire radiative power (FRP) estimates in boreal forests (also see Figure 6e). The left panel shows VIIRS fire frequency varying with VIIRS FRP (per fire pixel), and the right panel is MODIS fire frequency in five FRP ranges: 0–50, 51–100, 101–300, 301–600, 601–1,000, and 1,001–2,000 MW. Numbers on bars are the detection count in each range bin.

because the large MODIS pixels at off nadir could contain more fire events or areas, whereas VIIRS pixel size is smaller with fewer fire areas. However, VIIRS FRP is larger overall than MODIS FRP across swath, which is attributed to the fact that VIIRS with a smaller pixel size can detect more small fires than MODIS.

The FRP differences between MODIS and VIIRS are also attributed to the differences in sensor spectral bands and satellite overpass time. The impact of the difference in their spectral bands is demonstrated in the cluster FRP comparison. The carefully extracted fire clusters, after minimizing the differences in overpass time and VZA between MODIS and VIIRS data, provide FRP comparisons of individual fire events in different ecosystems globally. The relationship between the cluster MODIS and VIIRS FRP estimates is significant with a difference of 1% in croplands and savannas and less than 13% in broadleaf forests and rainforests. In boreal forests, however, the cluster MODIS FRP is as much as 47% higher than VIIRS FRP in intensive fire events (cluster FRP > 1,000 MW; Figure 6e) where FRP retrievals in nine MODIS fire detections range from 600 to 2,000 MW but VIIRS FRP in all fire detections is less than 600 MW (Figure 11). The underestimation of VIIRS FRP in large boreal forest fires is likely associated with the attenuation of VIIRS FRP by thick smoke plumes because the 4- μm VIIRS M-band has a wider wavelength that contains an important carbon dioxide (CO_2) absorption window than the 4- μm MODIS band (Giglio, Schroeder, & Justice, 2016). As a result, the increased atmospheric attenuation leads to underestimation of VIIRS FRP and the magnitude of FRP underestimation could be substantial when CO_2 -rich smoke plumes block the sensor's instantaneous field of view (Giglio, Schroeder, & Justice, 2016). This impact has been reported in a previous study, indicating that the absorption of infrared radiation by CO_2 in smoke plumes could result in a 10%–20% underestimation of VIIRS FRP (Oliva & Schroeder, 2015). Indeed, the larger the fire events (clusters), the heavier the smoke, which results in much stronger impacts on VIIRS FRP retrievals. However, the effect of smoke on VIIRS FRP could be very complex, which is likely associated with smoke thickness, plume height, etc. This result suggests that VIIRS FRP estimation could be improved with the atmospheric correction in the 4- μm band, particularly for large fires.

The temporal gap between the overpass time of VIIRS and MODIS, which spans from a few seconds to 50 min, has a twofold influence on their FRP difference. First, fire events, particularly small fires and fast spreading fires, could differ greatly during the period between the VIIRS and MODIS overpass times. This impact is demonstrated in agricultural fires in Punjab, India, on 11 November 2016 (Figure 12), where the overpass time of Aqua MODIS was merely 15 min earlier than that of VIIRS. The large discrepancy between MODIS and VIIRS fire detections is likely because the burning periods in individual agriculture fires are very short (Baucum et al., 2002). In other words, fires detected by one sensor could have gone out at the overpass of another sensor.

Second, during days when the temporal gaps are relatively long (e.g., >20 min), the associated cloud variation is likely one of the sources that complicate the FRP relationship between MODIS and VIIRS fire detections,

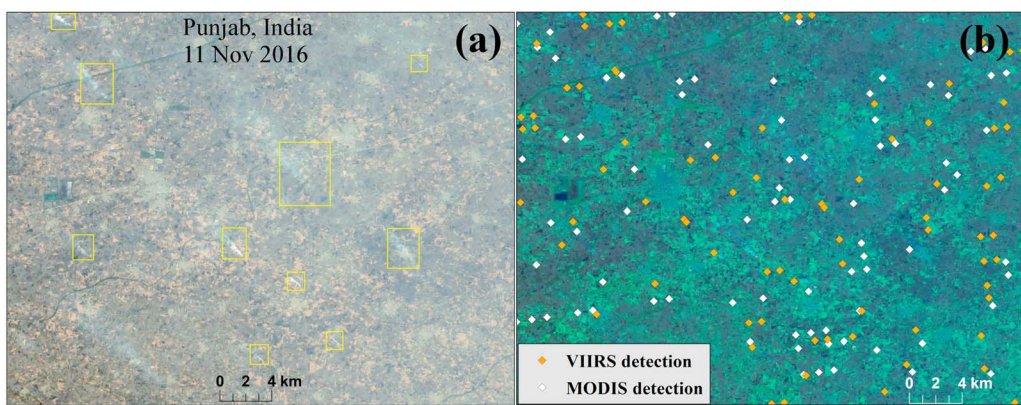


Figure 12. Active fire detections from Moderate Resolution Imaging Spectroradiometer (MODIS) and Visible Infrared Imaging Radiometer Suite (VIIRS) in croplands of Punjab, India, on 11 November 2016. MODIS and VIIRS flew over this area at 08:10 and 08:25 UTC, respectively. (a) The false-color composite of Landsat 8 band 4 (red), band 3 (green), and band 2 (blue). Landsat 8 collected this data at 05:31 UTC. Smoke plumes (in white delineated by the yellow rectangles) from agricultural burning were spreading toward the upper left direction. (b) Fire detections, for visualization purpose, were overlaid on the false-color composite image of Landsat 8 band 7 (red), band 5 (green), and band 3 (blue).

particularly in some tropical regions. Such impacts of cloud cover have been demonstrated in previous research that shows approximately 11% of omission error in MODIS fire detections caused by cloud obscuration in the Amazon basin compared to fire data from the Geostationary Operational Environmental Satellite (Schroeder et al., 2008).

The continental-scale FRP comparison based on the contemporaneous fire detections sensed by MODIS and VIIRS is less likely affected by the overpass temporal gap. As a result, MODIS and VIIRS FRP estimates are very similar, although some slight differences exist. This discrepancy could be explained by the higher capability of VIIRS in detecting smaller and cooler fires than the MODIS sensor. For instance, the continental-scale VIIRS FRP estimates are overall larger than MODIS FRP in savanna fire dominated Africa (Figure 7d) and agriculture fire dominated Europe (Figure 7c). However, this advantage could be offset by the attenuation of VIIRS FRP by CO₂-rich smoke plumes in some large fire regions (e.g., Asia in Figure 7e).

At the global grid cells and latitude average, discrepancies between MODIS and VIIRS FRP estimates could be attributed to most above-discussed factors because all fire detections from MODIS and VIIRS during the period from April 2016 to March 2017 were used to calculate the VIIRS-to-MODIS FRP ratio. In addition to the factors mentioned above, the sensor's swath width (Table 1) also matters in low latitudes. In tropical regions, the grid cell VIIRS FRP estimate is larger than MODIS FRP in most areas (e.g., Africa; Figure 9), which could be mostly explained by the omission error of MODIS fire data due to spatial coverage gaps between adjacent orbits at low latitudes (30°S and 30°N; see Figure 1; Wolfe et al., 2013). The MODIS omission error in the interorbital gaps has been demonstrated in fire detection (Cheng et al., 2013; Giglio et al., 2009) and emissions estimation (Wiedinmyer et al., 2011). Nevertheless, the larger MODIS FRP than VIIRS FRP in grid cells over South American tropical rainforests, as shown in Figure 9b, suggests that a combination of multiple factors could have very complex impacts on the discrepancies between MODIS and VIIRS FRP estimates.

6. Conclusions

This study examined the capability of Aqua MODIS and Suomi NPP VIIRS sensors in fire detection and characterization along satellite view angles and investigated the relationship between MODIS FRP and VIIRS FRP estimates at different spatial scales. The results indicate that MODIS detection capability decreases as view angle increases from nadir to the scan edge, whereas VIIRS experiences a generally consistent detection capability from all view angles. As a result, FRP per detection across swath increases greatly in MODIS but only slightly in VIIRS retrievals. This is mainly due to the sensing geometry difference between the two sensors. FRP comparisons at fire clusters and continental to global scales revealed that the relationship between MODIS and VIIRS FRP retrievals varies across ecosystems and spatial scales. The FRP relationship in individual fire events shows that cluster FRP estimates are overall comparable in savannas, croplands, and tropical rainforests and broadleaf forests. However, VIIRS FRP is much smaller than MODIS FRP for large fires in boreal

forests. The continental-scale FRP between contemporaneous MODIS and VIIRS fire detections is strongly correlated (Pearson's $r \geq 0.98$) in all six continents although VIIRS FRP is slightly larger. The grid-FRP difference between the two sensors is, on average, approximately 20% in most fire-prone regions, although it varies considerably in fire-limited regions. Generally, VIIRS FRP at grid cells is larger than MODIS FRP in savanna and agricultural fires but is smaller in tropical rainforests in South America and especially in boreal forests in North America and Eurasia. Along latitudes, VIIRS FRP is, on average, approximately 16% larger than MODIS FRP in the tropical zone (30°S – 30°N) where over 88% of VIIRS and MODIS fires is mainly distributed. At middle-to-high latitudes, VIIRS FRP is mostly less than MODIS FRP, particularly in boreal forests (55°N – 70°N). The larger VIIRS FRP estimates in small fires are generally attributed to the higher capability of detecting small and cool fires relative to MODIS estimates, whereas the lower VIIRS FRP in large and intensive fires, such as boreal forest fires, is likely associated with the attenuation of FRP by CO₂-rich smoke plumes associated with wider wavelength for VIIRS fire detections. Therefore, future work on atmospheric correction is expected to mitigate the underestimation of VIIRS FRP in these regions. In addition, interorbit gaps in MODIS observations at low latitudes could result in the underestimates of MODIS FRP.

The similarities of and discrepancies between MODIS and VIIRS FRP are associated with several other factors. VIIRS data have fewer duplicate fire detections than MODIS data. The FRP estimates from the interscan duplicate fire detections account for 18.3% overall in MODIS FRP, but 6.7% in VIIRS FRP. The interorbital duplicate detections exert very limited effects on FRP estimates, which is less than 1.3% of FRP. Moreover, the variations of cloudiness and small fires during the period between MODIS and VIIRS overpass times can also result in the discrepancy of FRP estimates.

In summary, the VIIRS sensor offers a good continuity to MODIS fire detections and FRP data record and provides a superior capability to detect smaller fires with no notable dependence on VZA. Users integrating current VIIRS 750-m active fire product into current applications that use MODIS active fire products should pay attention to the advantages and shortcomings of VIIRS sensor (M-bands) and active fire product. In addition, applications could also consider the VIIRS 375-m fire product (Schroeder et al., 2014), which is currently being evaluated for NOAA operational production. Finally, it should be noted that although the NOAA VIIRS NDEAF-L2 fire product provides timely or near-real-time fire observations based on the operational VIIRS Sensor Data Records, the NASA VIIRS fire products are transitioning to use better calibrated (or reprocessed) upstream data (Schroeder & Giglio, 2017).

Acknowledgments

This research was funded by NOAA contracts NA14NES4320003 and BG-133E-15-SE-1613. The authors thank three anonymous reviewers for constructive comments. Thanks also go to Wilfrid Schroeder for discussions in particular on VIIRS FRP retrieval issues. The manuscript contents are solely the opinions of the author(s) and do not constitute a statement of policy, decision, or position on behalf of NOAA or the U.S. Government. The authors comply with AGU's data policy. The raw input datasets (Aqua MODIS C6 MYD14 and MYD03, and Suomi NPP VIIRS NDEAF-L2 and GMTCO) used in this study are available for the public at NASA's Level-1 and Atmosphere Archive and Distribution System (LAADS; <https://ladsweb.modaps.eosdis.nasa.gov/>) and the NOAA Comprehensive Large Array-Data Stewardship System (CLASS; <https://www.class.ncdc.noaa.gov/>). The output data sets of this study are accessible at the institutional repository of South Dakota State University (https://openprairie.sdsstate.edu/global_land_surface_season_data/2/).

References

- Archibald, S., Lehmann, C. E. R., Gómez-Dans, J. L., & Bradstock, R. A. (2013). Defining pyromes and global syndromes of fire regimes. *Proceedings of the National Academy of Sciences*, 110(16), 6442–6447. <https://doi.org/10.1073/pnas.1211466110>
- Baucum, L., Rice, R., & Schueneman, T. (2002). An overview of Florida sugarcane, Agronomy Department, Florida Cooperative Extension Service, Institute of Food and Agricultural Sciences, University of Florida. Publication# SS-AGR-232. Retrieved from http://hendry.ifas.ufl.edu/pdfs/overview_of_florida_sugarcane.pdf. (last access on 08/07/2017).
- Boersma, K. F., Jacob, D. J., Trainic, M., Rudich, Y., DeSmedt, I., Dirksen, R., & Eskes, H. J. (2009). Validation of urban NO₂ concentrations and their diurnal and seasonal variations observed from the SCIAMACHY and OMI sensors using in situ surface measurements in Israeli cities. *Atmospheric Chemistry and Physics*, 9(12), 3867–3879. <https://doi.org/10.5194/acp-9-3867-2009>
- Cao, C., Luccia, F. J. D., Xiong, X., Wolfe, R., & Weng, F. (2014). Early on-orbit performance of the Visible Infrared Imaging Radiometer Suite onboard the Suomi National Polar-Orbiting Partnership (S-NPP) satellite. *IEEE Transactions on Geoscience and Remote Sensing*, 52(2), 1142–1156. <https://doi.org/10.1109/TGRS.2013.2247768>
- Cheng, D., Rogan, J., Schneider, L., & Cochrane, M. (2013). Evaluating MODIS active fire products in subtropical Yucatán forest. *Remote Sensing Letters*, 4(5), 455–464. <https://doi.org/10.1080/2150704X.2012.749360>
- Cohen, W. B., Maiersperger, T. K., Gower, S. T., & Turner, D. P. (2003). An improved strategy for regression of biophysical variables and Landsat ETM+ data. *Remote Sensing of Environment*, 84(4), 561–571. [https://doi.org/10.1016/S0034-4257\(02\)00173-6](https://doi.org/10.1016/S0034-4257(02)00173-6)
- Csizsar, I., Schroeder, W., Giglio, L., Ellicott, E., Vadrevu, K. P., Justice, C. O., & Wind, B. (2014). Active fires from the Suomi NPP Visible Infrared Imaging Radiometer Suite: Product status and first evaluation results. *Journal of Geophysical Research: Atmospheres*, 119, 803–816. <https://doi.org/10.1002/2013JD020453>
- Csizsar, I., Schroeder, W., Giglio, L., Mikles, V., & Tsidulko, M. (2016). The NOAA NDE Active Fire EDR External Users Manual. Retrieved from https://www.star.nesdis.noaa.gov/jpss/documents/UserGuides/VIIRS_ActiveFire_EUM.pdf. (last accessed on 1/20/2018).
- Darmenov, A. S., & Silva, A. D. (2015). The Quick Fire Emissions Dataset (QFED): Documentation of versions 2.1, 2.2 and 2.4 rep. TM-2015-104606, 212 pp, NASA, Goddard Space Flight Center greenbelt, MD.
- Ellicott, E., Vermote, E., Giglio, L., & Roberts, G. (2009). Estimating biomass consumed from fire using MODIS FRE. *Geophysical Research Letters*, 36, L13401. <https://doi.org/10.1029/2009GL038581>
- Flannigan, M. D., & Haar, T. H. V. (1986). Forest fire monitoring using NOAA satellite AVHRR. *Canadian Journal of Forest Research*, 16(5), 975–982. <https://doi.org/10.1139/x86-171>
- Freeborn, P. H., Jolly, W. M., & Cochrane, M. A. (2016). Impacts of changing fire weather conditions on reconstructed trends in U.S. wildland fire activity from 1979 to 2014. *Journal of Geophysical Research: Biogeosciences*, 121, 2856–2876. <https://doi.org/10.1002/2016JG003617>

- Freeborn, P. H., Wooster, M. J., Roberts, G., Malamud, B. D., & Xu, W. (2009). Development of a virtual active fire product for Africa through a synthesis of geostationary and polar orbiting satellite data. *Remote Sensing of Environment*, 113(8), 1700–1711. <https://doi.org/10.1016/j.rse.2009.03.013>
- Freeborn, P. H., Wooster, M. J., Roy, D. P., & Cochrane, M. A. (2014). Quantification of MODIS fire radiative power (FRP) measurement uncertainty for use in satellite-based active fire characterization and biomass burning estimation. *Geophysical Research Letters*, 41, 1988–1994. <https://doi.org/10.1002/2013GL059086>
- Friedl, M. A., Sulla-Menashe, D., Tan, B., Schneider, A., Ramankutty, N., Sibley, A., & Huang, X. (2010). MODIS Collection 5 global land cover: Algorithm refinements and characterization of new datasets. *Remote Sensing of Environment*, 114(1), 168–182. <https://doi.org/10.1016/j.rse.2009.08.016>
- Giglio, L., Csiszar, I., & Justice, C. O. (2006). Global distribution and seasonality of active fires as observed with the Terra and Aqua Moderate Resolution Imaging Spectroradiometer (MODIS) sensors. *Journal of Geophysical Research*, 111, G02016. <https://doi.org/10.1029/2005JG000142>
- Giglio, L., Descloitres, J., Justice, C. O., & Kaufman, Y. J. (2003). An enhanced contextual fire detection algorithm for MODIS. *Remote Sensing of Environment*, 87(2–3), 273–282. [https://doi.org/10.1016/S0034-4257\(03\)00184-6](https://doi.org/10.1016/S0034-4257(03)00184-6)
- Giglio, L., Loboda, T., Roy, D. P., Quayle, B., & Justice, C. O. (2009). An active-fire based burned area mapping algorithm for the MODIS sensor. *Remote Sensing of Environment*, 113(2), 408–420. <https://doi.org/10.1016/j.rse.2008.10.006>
- Giglio, L., Schroeder, W., Csiszar, I., & Tsidliko, M. (2016). Algorithm theoretical basis document for NOAA NDE VIIRS active fire. Retrieved from https://www.star.nesdis.noaa.gov/jpss/documents/ATBD/ATBD_NDE_AF_v2.6.pdf. (last accessed on 6/2/2017).
- Giglio, L., Schroeder, W., & Justice, C. O. (2016). The collection 6 MODIS active fire detection algorithm and fire products. *Remote Sensing of Environment*, 178, 31–41. <https://doi.org/10.1016/j.rse.2016.02.054>
- Goldberg, M. D., Kilcoyne, H., Cikanek, H., & Mehta, A. (2013). Joint Polar Satellite System: The United States next generation civilian polar-orbiting environmental satellite system. *Journal of Geophysical Research*, 118, 13,463–13,475. <https://doi.org/10.1002/2013JD020389>
- Ichoku, C., Ellison, L. T., Willmot, K. E., Matsui, T., Dezfuli, A. K., Gatebe, C. K., et al. (2016). Biomass burning, land-cover change, and the hydrological cycle in Northern sub-Saharan Africa. *Environmental Research Letters*, 11(9), 095005. <https://doi.org/10.1088/1748-9326/11/9/095005>
- Ichoku, C., Giglio, L., Wooster, M. J., & Remer, L. A. (2008). Global characterization of biomass-burning patterns using satellite measurements of fire radiative energy. *Remote Sensing of Environment*, 112(6), 2950–2962. <https://doi.org/10.1016/j.rse.2008.02.009>
- Ichoku, C., & Kaufman, Y. J. (2005). A method to derive smoke emission rates from MODIS fire radiative energy measurements. *Geoscience and Remote Sensing, IEEE Transactions on*, 43(11), 2636–2649. <https://doi.org/10.1109/TGRS.2005.857328>
- Kaiser, J. W., Heil, A., Andreea, M. O., Benedetti, A., Chubarova, N., Jones, L., et al. (2012). Biomass burning emissions estimated with a global fire assimilation system based on observed fire radiative power. *Biogeosciences*, 9(1), 527–554. <https://doi.org/10.5194/bg-9-527-2012>
- Kaufman, Y. J., Justice, C. O., Flynn, L. P., Kendall, J. D., Prins, E. M., Giglio, L., et al. (1998). Potential global fire monitoring from EOS-MODIS. *Journal of Geophysical Research*, 103, 32,215–32,238. <https://doi.org/10.1029/98JD01644>
- Kumar, S. S., Roy, D. P., Boschetti, L., & Kremens, R. (2011). Exploiting the power law distribution properties of satellite fire radiative power retrievals: A method to estimate fire radiative energy and biomass burned from sparse satellite observations. *Journal of Geophysical Research*, 116, D19303. <https://doi.org/10.1029/2011JD015676>
- Oliva, P., & Schroeder, W. (2015). Atmospheric correction of VIIRS and MODIS fire radiative power retrievals for multi-sensor comparison, paper presented at 2015 IEEE International Geoscience and Remote Sensing Symposium (IGARSS), 26–31 July 2015.
- Peterson, D., Wang, J., Ichoku, C., Hyer, E., & Ambrosia, V. (2013). A sub-pixel-based calculation of fire radiative power from MODIS observations: 1: Algorithm development and initial assessment. *Remote Sensing of Environment*, 129, 262–279. <https://doi.org/10.1016/j.rse.2012.10.036>
- Prins, E. M., & Menzel, W. P. (1992). Geostationary satellite detection of bio mass burning in South America. *International Journal of Remote Sensing*, 13(15), 2783–2799. <https://doi.org/10.1080/01431169208904081>
- Roberts, G., Wooster, M. J., Xu, W., Freeborn, P. H., Morcrette, J. J., Jones, L., et al. (2015). LSA SAF Meteosat FRP products—Part 2: Evaluation and demonstration for use in the Copernicus Atmosphere Monitoring Service (CAMS). *Atmospheric Chemistry and Physics*, 15(22), 13,241–13,267. <https://doi.org/10.5194/acp-15-13241-2015>
- Roberts, G. J., & Wooster, M. J. (2008). Fire detection and fire characterization over Africa using Meteosat SEVIRI. *Geoscience and Remote Sensing, IEEE Transactions on*, 46(4), 1200–1218. <https://doi.org/10.1109/TGRS.2008.915751>
- Roy, D. P., & Kumar, S. S. (2017). Multi-year MODIS active fire type classification over the Brazilian Tropical Moist Forest Biome. *International Journal of Digital Earth*, 10(1), 54–84. <https://doi.org/10.1080/17538947.2016.1208686>
- Schroeder, W., Csiszar, I., & Morisette, J. (2008). Quantifying the impact of cloud obscuration on remote sensing of active fires in the Brazilian Amazon. *Remote Sensing of Environment*, 112(2), 456–470. <https://doi.org/10.1016/j.rse.2007.05.004>
- Schroeder, W., & Giglio, L. (2017). Visible Infrared Imaging Radiometer Suite (VIIRS) 750 m Active Fire Detection and Characterization Algorithm Theoretical Basis Document 1.0. Retrieved from https://viirsland.gsfc.nasa.gov/PDF/VIIRS_Activefire_ATBD750_v1.pdf. (last accessed on 1/20/2018).
- Schroeder, W., Oliva, P., Giglio, L., & Csiszar, I. A. (2014). The new VIIRS 375 m active fire detection data product: Algorithm description and initial assessment. *Remote Sensing of Environment*, 143, 85–96. <https://doi.org/10.1016/j.rse.2013.12.008>
- Smith, A. M. S., & Wooster, M. J. (2005). Remote classification of head and backfire types from MODIS fire radiative power and smoke plume observations. *International Journal of Wildland Fire*, 14(3), 249–254. <https://doi.org/10.1071/WF05012>
- Smith, R. J. (2009). Use and misuse of the reduced major axis for line-fitting. *American Journal of Physical Anthropology*, 140(3), 476–486. <https://doi.org/10.1002/ajpa.21090>
- Vermote, E., Ellicott, E., Dubovik, O., Lapyonok, T., Chin, M., Giglio, L., & Roberts, G. J. (2009). An approach to estimate global biomass burning emissions of organic and black carbon from MODIS fire radiative power. *Journal of Geophysical Research*, 114, D18205. <https://doi.org/10.1029/2008JD011188>
- White, M. A., De Beurs, K. M., Didan, K., Inouye, D. W., Richardson, A. D., Jensen, O. P., et al. (2009). Intercomparison, interpretation, and assessment of spring phenology in North America estimated from remote sensing for 1982–2006. *Global Change Biology*, 15(10), 2335–2359. <https://doi.org/10.1111/j.1365-2486.2009.01910.x>
- Wiedinmyer, C., Akagi, S. K., Yokelson, R. J., Emmons, L. K., Al-Saadi, J. A., Orlando, J. J., & Soja, A. J. (2011). The Fire INventory from NCAR (FINN): A high resolution global model to estimate the emissions from open burning. *Geoscientific Model Development*, 4(3), 625–641. <https://doi.org/10.5194/gmd-4-625-2011>
- Wolfe, R. E., Lin, G., Nishihama, M., Tewari, K. P., Tilton, J. C., & Isaacman, A. R. (2013). Suomi NPP VIIRS prelaunch and on-orbit geometric calibration and characterization. *Journal of Geophysical Research: Atmospheres*, 118, 11,508–11,521. <https://doi.org/10.1002/jgrd.50873>

- Wolfe, R. E., Nishihama, M., Fleig, A. J., Kuyper, J. A., Roy, D. P., Storey, J. C., & Patt, F. S. (2002). Achieving sub-pixel geolocation accuracy in support of MODIS land science. *Remote Sensing of Environment*, 83(1–2), 31–49. [https://doi.org/10.1016/S0034-4257\(02\)00085-8](https://doi.org/10.1016/S0034-4257(02)00085-8)
- Wolfe, R. E., Roy, D. P., & Vermote, E. (1998). MODIS land data storage, gridding, and compositing methodology: Level 2 grid. *Geoscience and Remote Sensing, IEEE Transactions on*, 36(4), 1324–1338. <https://doi.org/10.1109/36.701082>
- Wooster, M. J., Roberts, G., Freeborn, P. H., Xu, W., Govaerts, Y., Beeby, R., et al. (2015). LSA SAF Meteosat FRP products—Part 1: Algorithms, product contents, and analysis. *Atmospheric Chemistry and Physics*, 15(22), 13,217–13,239. <https://doi.org/10.5194/acp-15-13217-2015>
- Wooster, M. J., & Zhang, Y. H. (2004). Boreal forest fires burn less intensely in Russia than in North America. *Geophysical Research Letters*, 31, L20505. <https://doi.org/10.1029/2004GL020805>
- Wooster, M. J., Zhukov, B., & Oertel, D. (2003). Fire radiative energy for quantitative study of biomass burning: Derivation from the BIRD experimental satellite and comparison to MODIS fire products. *Remote Sensing of Environment*, 86(1), 83–107. [https://doi.org/10.1016/S0034-4257\(03\)00070-1](https://doi.org/10.1016/S0034-4257(03)00070-1)
- Zhang, X., Kondragunta, S., Da Silva, A., Lu, S., Kim, H., Ding, H., Zhu, Y., & Cheng, Z. (2014). Algorithm theoretical basis document for NOAA GBBEPx emissions product, version 1.1, edited, NOAA/NESDIS/STAR. Retrieved from http://www.ospo.noaa.gov/Products/land/gbbepx/docs/GBBEPx_ATBD.pdf. (last accessed on 1/8/2018).
- Zhang, X., Kondragunta, S., Ram, J., Schmidt, C., & Huang, H.-C. (2012). Near-real-time global biomass burning emissions product from geostationary satellite constellation. *Journal of Geophysical Research*, 117, D14201. <https://doi.org/10.1029/2012JD017459>